Title

Feasibility of deriving a novel imaging biomarker based on patient-specific lung elasticity for characterizing the degree of COPD in lung SBRT patients

Journal

British Journal of Radiology, 92(1094)

ISSN

0007-1285

Authors

Hasse, Katelyn
Neylon, John
Min, Yugang
et al.

Publication Date

2019-02-01

DOI

10.1259/bjr.20180296

Peer reviewed

BJR

https://doi.org/10.1259/bjr.20180296

Received: 21 March 2018 | Revised: 19 September 2018 | Accepted: 01 October 2018

Cite this article as:
Hasse K, Neylon J, Min Y, O'Connell D, Lee P, Low DA, et al. Feasibility of deriving a novel imaging biomarker based on patient-specific lung elasticity for characterizing the degree of COPD in lung SBRT patients. *Br J Radiol* 2019; **91**: 20180296.

FULL PAPER

Feasibility of deriving a novel imaging biomarker based on patient-specific lung elasticity for characterizing the degree of COPD in lung SBRT patients

KATELYN HASSE, Ph.D., JOHN NEYLON, PhD, YUGANG MIN, PhD, DYLAN O'CONNELL, PhD, PERCY LEE, MD, DANIEL A LOW, PhD and ANAND P SANTHANAM, PhD

Departmentof Radiation Oncology, University of California, Los Angeles Medical Plaza Driveway, Los Angeles, CA, US

Address correspondence to: Ms Katelyn Hasse
E-mail: *katelyn.hasse@ucsf.edu*

Objective: Lung tissue elasticity is an effective spatial representation for Chronic Obstructive Pulmonary Disease phenotypes and pathophysiology. We investigated a novel imaging biomarker based on the voxel-by-voxel distribution of lung tissue elasticity. Our approach combines imaging and biomechanical modeling to characterize tissue elasticity.

Methods: We acquired 4DCT images for 13 lung cancer patients with known COPD diagnoses based on GOLD 2017 criteria. Deformation vector fields (DVFs) from the deformable registration of end-inhalation and end-exhalation breathing phases were taken to be the ground-truth. A linear elastic biomechanical model was assembled from end-exhalation datasets with a density-guided initial elasticity distribution. The elasticity estimation was formulated as an iterative process, where the elasticity was optimized based on its ability to reconstruct the ground-truth. An imaging biomarker (denoted YM_{1-3}) derived from the optimized elasticity distribution, was compared with the current gold standard, RA_{950} using confusion matrix and area under the receiver operating characteristic (AUROC) curve analysis.

Results: The estimated elasticity had 90 % accuracy when representing the ground-truth DVFs. The YM_{1-3} biomarker had higher diagnostic accuracy (86% *vs* 71 %), higher sensitivity (0.875 *vs* 0.5), and a higher AUROC curve (0.917 *vs* 0.875) as compared to RA_{950}. Along with acting as an effective spatial indicator of lung pathophysiology, the YM_{1-3} biomarker also proved to be a better indicator for diagnostic purposes than RA_{950}.

Conclusions: Overall, the results suggest that, as a biomarker, lung tissue elasticity will lead to new end points for clinical trials and new targeted treatment for COPD subgroups.

Advances in knowledge: The derivation of elasticity information directly from 4DCT imaging data is a novel method for performing lung elastography. The work demonstrates the need for a mechanics-based biomarker for representing lung pathophysiology.

INTRODUCTION

Chronic Obstructive Pulmonary Disease (COPD) refers to a large group of progressive lung diseases that are characterized by persistent reduction of airflow which inhibits normal breathing.[1] Despite the heterogeneity of COPD phenotypes, diagnosis is based on symptoms and presence of fixed airflow obstruction, which do not fully reflect the heterogeneous pathophysiological conditions observed in COPD.[2,3] There is an emerging role for quantitative computed tomography (CT) to assess lung structure and function in the evaluation of pulmonary emphysema.[4,5] A common method employed for the detection and quantification of the lung function is lung densitometry, where voxels on full inspiration lung CT scans with less than −950HU are classified as emphysematous tissue; this is measured by the relative area of voxels less than −950 HU and known as RA_{950}.[6,7] The percent of voxels on full expiration lung CT scans with less than −856 HU have been related to gas trapping.[8] CT densitometry has been observed to relate well to clinical parameters observed in a recent systematic review and other studies.[9–11] Recently, imaging post-processing and registration techniques have been evaluated for linking inspiratory and expiratory CT lung scans to provide a classification of individual parenchymal voxels within COPD phenotypes such as emphysema, gas-trapping, and small airways disease.[8,12,13] However, a clear limitation of these methods stems from the fact that COPD pathophysiology is related to changes in the tissue mechanics, which may not be fully represented by either a single quantitative CT or post-processing image pairs.[14]

Although these techniques are promising, there is a need to further characterize COPD pathophysiology by considering the lung tissue mechanics. Lung function is closely related to the mechanical properties of the lung parenchyma.[15] COPD is characterized by damaged lung tissues with altered mechanical properties and ventilation profiles.[16] For example, the destruction of collagen and elastin fibers in emphysematous tissue decreases the strength and elastic recoil of the tissue, subsequently reducing the elastic modulus.[17] The dynamic mechanical properties of the lung and the transformation during disease is generally appreciated within the field of clinical pulmonary research.[18] Although the link between lung mechanics and disease initiation and progression has been established, the ability to noninvasively assess disease progression through mechanical property changes at a regional level has not been investigated. A key biomechanical property of tissue is its elasticity. Elastography is a non-invasive imaging technique for quantifying the elasticity distribution in tissues. Elastography techniques can provide contrast between the mechanical properties of normal and diseased tissue. Currently, elastography exists across several modalities including MR and ultrasound.[19] The air within and motion of the lungs renders conventional elastography techniques difficult to implement.[20] In addition, elastography has not yet been fully investigated for COPD patients.

4DCT images are pertinent for lung elastography as they encapsulate lung tissue motion during tidal breathing.[21] 4DCT data acquisition involves CT imaging in axial cine mode with retrospective image sorting based on respiratory phase.[22] 4DCT images are also routinely acquired for lung cancer patients that receive radiation therapy.[23] Since a significant portion of lung cancer patients also have some level of COPD, analyzing their 4DCT images for lung elastography could yield critical information regarding the lung tissue elasticity for COPD affected regions. The result of such lung elastography is novel for the field of COPD diagnosis and treatment.

METHODS AND MATERIALS

In this article, we present a 4DCT-based lung elastography procedure for evaluating lung tissue elasticity in COPD affected lungs. We further correlate the spatial distribution of lung tissue elasticity with the inherent GOLD severity criteria and RA_{950} to validate the diagnostic and staging ability of the lung tissue elasticity. Using the estimated elasticity, we investigated a novel imaging biomarker, YM_{1-3}. The results presented in this article support our hypothesis that lung tissue elasticity could lead to an effective biomarker for characterizing spatial lung pathophysiological changes and its heterogeneity can be used for the quantitative evaluation of functional lung regions. In addition, the biomarker presented in this article performs better than RA_{950}, thereby demonstrating the potential for mechanics-derived elasticity as a biomarker for COPD.

Data

A set of 13 lung cancer SBRT patient 4DCT datasets were retrospectively obtained using a novel protocol designed to mitigate image artifacts at UCLA from October 2012 to August 2016.[24] The patient datasets were acquired with patient consent and approval from the Institutional Review Board of UCLA (IRB #11–000620-CR-00004). The 4DCT scans were acquired pre-treatment with the same acquisition protocol on Siemens Definition Flash, Siemens Biograph 64, and Siemens Definition AS 64 scanners and reconstructed with 1 mm slice thikceness using the Siemens reconstruction kernel B30f. The protocol required approximately 2.5 s to scan the entire lung volume from apices to lung base.[25] The pulmonary tissue was segmented using an intensity thresholding approach.[26] Pulmonary function tests were available for all 13 of the patients.

Elastography

Biomechanical model

The primary aim of the lung elasticity evaluation for COPD patients was to determine if patient disease status could be correlated with underlying tissue elasticity derived from the 4DCT geometry, boundary conditions, and the deformation vector fields. Peers have investigated characterizing lung function using only the deformation vector fields by computing the voxel-by-voxel expansion and contraction.[2] We envision that integrating the three above-mentioned components using a biomechanical framework will enable the precise characterization of lung tissue elasticity. A biomechanical model that has been well validated using head and neck, breast, and lung datasets was used as a forward model to solve the inverse elasticity problem.[24,27] Biomechanical property estimations are generated using iterative inverse deformation methods that use biomechanical models to estimate the linear elasticity that duplicates the image dataset deformations.[28] The geometry of the biomechanical model was instantiated using end-exhalation lung datasets, where every image voxel corresponded to a finite element within the model. For the estimation process, an initial density-guided linear elastic distribution was assigned to the biomechanical lung model, associating a discrete elasticity value to every lung tissue voxel. For each patient, end-inhalation and end-exhalation breathing phases were first registered using an in-house optical flow deformable image registration (DIR) algorithm.[29] The displacement of each voxel was taken to be the ground-truth.[25,29] The inverse elasticity problem was formulated as a parameter-optimization problem with an objective to determine the elasticity that would minimize the difference between the ground-truth displacement and that computed by the biomechanical model. The displacement of the lung boundary (between parenchymal and pleural tissues) obtained from the DIR algorithm were used as boundary condition for the elastography analysis to deform the biomechanical model to represent end-inhalation geometry. For changes in the lung boundary, the inner voxels biomechanically deformed according to the linear elastic forces within the biomechanical model. The Euclidean distance between the initial and final position for each voxel was taken to be the model deformation for that voxel.

Parameter optimization

A detailed description of the inverse elasticity estimation and underlying parameter estimation has been discussed in.[24] For clarity, we present a brief description of the parameter optimization process. Solving the inverse elasticity problem was carried out by (a) computing the displacement vector field for

every voxel of lung tissue for a given elasticity distribution (as discussed above), and (b) optimizing the elasticity distribution that best reproduced the ground-truth.[26] The tissue elasticity was iteratively updated and optimized and the resulting displacement was then compared with the ground-truth DIR displacement until convergence.[30]

Lung elasticity evaluation for COPD patients

To evaluate the correlation of disease status with underlying elasticity, the patients were first classified by an experienced physician with a score of 0–4 according to the GOLD 2017 standard, where 0 corresponds to no limitation and 4 to very severe airway limitation.[31] The physician had no prior knowledge of the elasticity metrics of the patients. The corresponding 4DCT patient datasets were used to estimate the tissue elasticity and assessed for their ability to discriminate patient COPD status with the following three experiments:

Experiment 1: Documenting spatial changes in the elasticity for COPD patients

It is expected that the elasticity should be spatially varying because COPD does not present homogeneously. We expect the elasticity distributions to vary widely between subjects. In addition, correlations between the tissue displacements and elasticity distributions were analyzed. We expect a poor correlation, since elasticity should be independent of the deformation. Correlations between intensity and elasticity distributions were also analyzed. The correlation between intensity and elasticity is expected to be high, as we want to compare our results to the intensity-derived RA_{950} metric. However, a perfect correlation would indicate that elasticity does not provide any more useful information than RA_{950}.

Experiment 2: Investigating changes in elasticity distribution for different stages of COPD patients

An increase in the GOLD criteria reflects a decrease in the lung function – these changes should be evident in the underlying elasticity. Parenchymal voxels were segmented using an intensity thresholding approach, where parenchymal voxels were taken to be those voxels with intensity values between −800 and −500 HU.[26] Average elasticity values for parenchymal tissue were correlated with the GOLD criteria to observe for any changes in the lung function. Elasticity histograms were generated for all GOLD scores and also analyzed for change in lung tissue function.

Experiment 3: Comparing an elasticity-derived biomarker to RA_{950}

While the elasticity estimation gives a distribution of values, for diagnostic purposes, it is convenient to have a binary indicator of disease. A binary COPD classification was first determined based on the GOLD score; a score of 0 or 1 corresponded to a non-COPD (normal) classification (value of 0) and a score greater than 2 corresponded to a COPD classification (value of 1).[32]

Using these classification methods, 9 of the patients that were included in this study were then classified as having COPD (GOLD 2–4). First, the voxel-to-voxel correlation of the elasticity with RA_{950} was investigated, to determine if the elasticity information could serve as a proxy for COPD, in this case specifically emphysema, diagnosis. For completeness, RA_{910}, RA_{960}, and RA_{970} were also investigated. Second, a binary elasticity threshold was empirically derived to discriminate patient COPD status. The relative area of voxels with an elasticity less than the binary elasticity threshold or Young's modulus, YM_{1-3}, was compared to the conventional RA_{950} imaging metric using a confusion matrix and ROC analysis.

Table 1. onvergence results of elasticity estimation study broken down by underlying tissue type

Patient ID	Convergence percentage of voxels < 10% maximum deformation (%)
1	92.85
2	89.32
3	94.11
4	94.70
5	78.75
6	85.51
7	85.63
8	94.30
9	92.47
10	89.18
11	90.61
12	92.82
13	87.08
Average	87.32

RESULTS

Overall, 89.35 ±8.16% of voxels converged within 10% of the deformation. Table 1 denotes the convergence percentage for each of the patients for parenchymal tissue. 87.32 ± 4.61% of parenchymal voxels converged within 10% of maximum deformation. The high convergence of the parenchymal tissue motivates the use of the elasticity results for the remainder of the experiments.

Experiment 1: Documenting spatial changes in elasticity for COPD patients

Figure 1 (a) shows the ground–truth displacement for a 2D slice of non-COPD patient lung, while Figure 1(b) shows the resultant elasticity distribution. Figure 1(c & d) show the ground-truth deformation and elasticity maps, respectively, for a COPD patient with impaired lung function. The patients shown here were chosen in such a way that their maximum ground-truth deformation values matched. However, the elasticity distributions differ significantly, demonstrating the ability of the proposed methods to discriminate normal versus diseased patients. The elasticity of the COPD patient Figure 1d is much lower than that of the non-COPD patient (Figure 1b), which was expected since COPD is known to affect elastin and collagen in diseased tissue,[17] leading to a decrease in strength

Figure 1. 2D slices showing ground-truth displacement (a & c) and reconstructed elasticity distributions (b & d) for normal (a & b) and COPD (c & d) patients respectively.

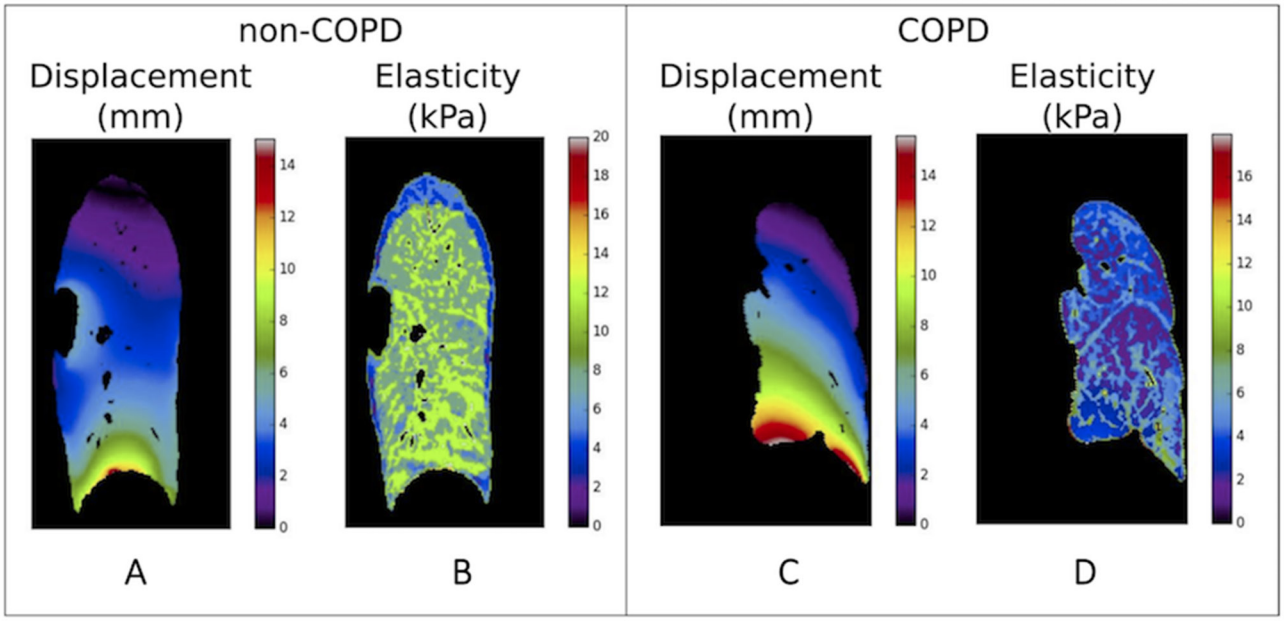

and elasticity. This supports the hypothesis that the elasticity estimation discussed here can provide useful functional information, which is explored in Experiment 2.

We now present the elasticity distribution as a function of the displacement magnitude as well as the voxel intensity. Table 2 denotes the correlation coefficient between both a) displacement and elasticity distributions and b) the intensity and elasticity distributions for each patient.

Table 2. Displacement and elasticity correlation along intensity and elasticity correlation results

Patient ID	Correlation between displacement and elasticity	Correlation between intensity and elasticity
1	0.14	0.76
2	0.02	0.78
3	0.03	0.61
4	0.12	0.87
5	0.02	0.91
7	0.11	0.69
7	0.08	0.83
8	0.04	0.89
9	0.22	0.26
10	0.06	0.80
11	0.02	0.86
12	0.11	0.72
13	0.15	0.85
Average	0.09	0.76

On average, the correlation between elasticity and displacement is low with a Pearson correlation coefficient of 0.09. The low correlation strongly suggests that elasticity is independent of the displacement. Therefore, deriving functional information solely from displacement-based metrics may not be a good representation of the underlying pathophysiology. The correlation between elasticity and intensity was better, with an average coefficient of 0.76. This supports the hypothesis that elasticity is related to intensity and can be used to complement intensity-derived metrics, such as RA_{950}, while still providing additional functional information. This will be further explored in Experiment 3.

Experiment 2: Investigating changes in elasticity distribution for different stages of COPD patients

Table 3 denotes maximum deformation and average elasticity, both for all lung tissue and parenchymal tissue only, for the patients stratified by GOLD score. It can be seen that, although maximum deformation did not have a correlation with the GOLD criteria, average elasticity varied with decreasing lung function. Furthermore, parenchymal average elasticity decreased with decreasing lung function, strongly suggesting that elasticity can provide functional lung information.

While average elasticity relates to a decrease in lung function, the average is a high-level representation the whole physiology. To evaluate whether the distribution of the elasticity information correlates with lung function, a histogram of the elasticity results for the groups of patients with GOLD status 0–4 is shown in Figure 2. The peak of elasticity for the patients with normal lung function (GOLD 0–1) is significantly further to the right than those patients with COPD (GOLD 2–4), which corresponds to the average elasticity values seen in Table 3 above. The histograms illustrate that the shift between non-COPD and COPD patients isn't gradual. Specifically, an increase in the GOLD status

Table 3. Maximum deformation and average elasticity for GOLD score groups of patients

Patient averages	Maximum deformation[33]	Average elasticity (kPa)	Average parenchymal elasticity (kPa)
All	17.52	6.24	5.87
GOLD 0	10.05	6.55	5.28
GOLD 1	18.30	6.79	7.28
GOLD 2	22.82	6.33	6.06
GOLD 3	19.19	4.32	4.34
GOLD 4	8.92	4.40	4.43

was characterized by an increase in the number of voxels with an elasticity between 1 and 3 kPa, and a significant decrease in the number of voxels with an elasticity between 4 and 8 kPa. This can be understood by the fact that COPD patients are known to have damaged lung tissue with decreased collagen and elastin content.

Using this information, we derived a novel elasticity-based imaging biomarker that represents the percentage of parenchymal voxels within 1–3 kPa. Specifically, a new mechanics-based imaging biomarker, YM_{1-3}, represents the percentage of voxels of parenchymal tissue with an elasticity between 1 and 3 kPa. The range of voxels with elasticity between 1 and 3 kPa, will be explored in Experiment 3 below.

Experiment 3: Comparing an elasticity-derived biomarker to RA_{950}

A visual representation of the RA_{950} imaging biomarker is shown along with the corresponding elastic modulus distributions in Figure 3. Figure 3 (a–e) show source CT images with HU values less than −950 HU highlighted in red, a visual approximation of RA_{950}. Figure 3 (f–j) show the corresponding elasticity distributions for the same slices. Slices are shown for patients with GOLD 0 (a, f) through GOLD 4 (e, j) status. It can be seen that the regions highlighted in red correspond to the lower elasticity regions in purple and dark blue. Furthermore, the prevalence of low intensity regions and the lowered elasticity regions increased with the GOLD status, illustrating that a decrease in the lung

Figure 2. Histogram of elasticity values for patients with GOLD scores ranging from 0 (top) to 4 (bottom).

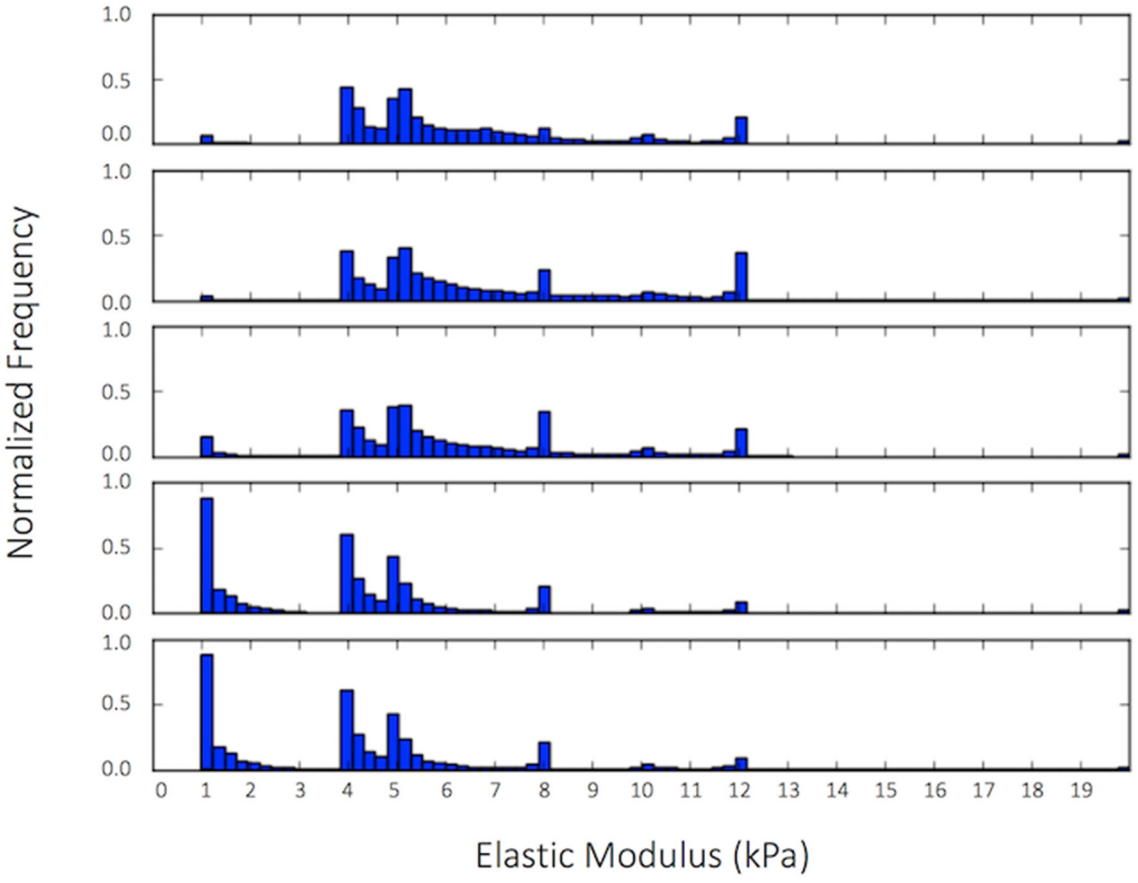

Figure 3. Illustration of source CT with HU values less than −950 HU highlighted in red shown for a GOLD 0 (a), GOLD 1 (b), GOLD 2 (c), GOLD 3 (d), and GOLD 4 (e) patient. Elasticity distributions for same patients are shown in (f–j).

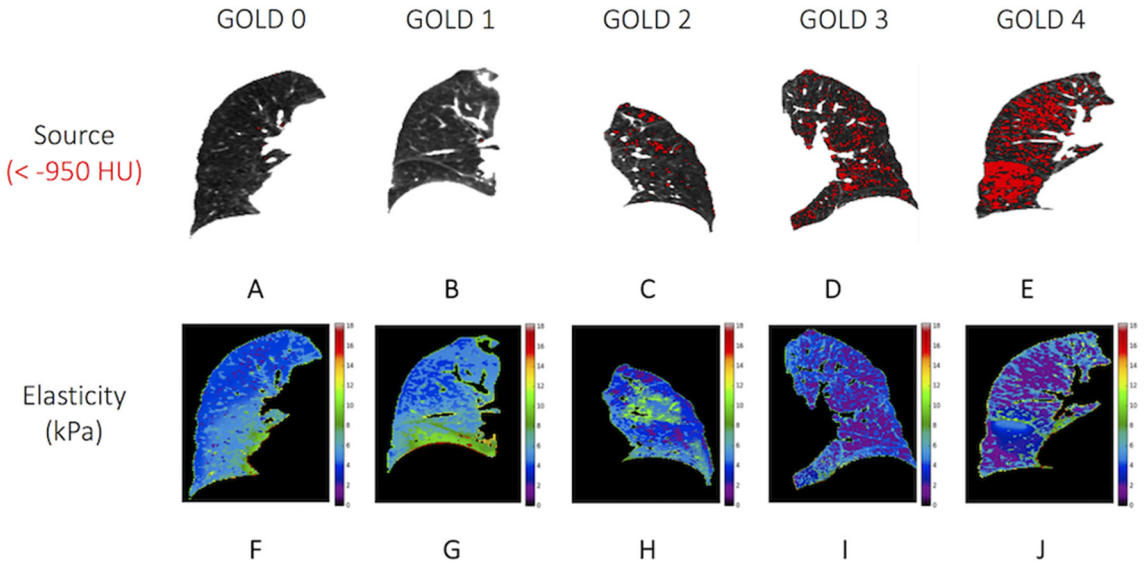

function corresponded with a decrease in both intensity and elasticity values. RA_{910}, RA_{960}, and RA_{970} were also investigated, and the same overall trends were observed.

The voxels with an elasticity between 1 and 3 kPa are compared to a visual representation of RA_{950} in Figure 4. Figure 4a depicts a source CT image with voxel intensity of less than −950 highlighted in red to illustrate RA_{950}. Figure 4b shows the reconstructed elasticity distribution, with voxel elasticity between 1 and 3 kPa also highlighted in red. These values were derived from the histogram in Figure 2. Many of the highlighted regions overlap between Figure 4a,b, demonstrating the potential of low elasticity values to be indicative of impaired lung function.

To further illustrate the diagnostic potential of an elasticity COPD metric, a confusion matrix was used to compare the diagnostic capabilities of YM_{1-3} versus RA_{950} and is shown for each metric respectively in Figure 5 below.

Figure 4. The conventional RA_950 imaging metric and an initial elasticity derived imaging metric for the same 2-D slice of a patient left lung.

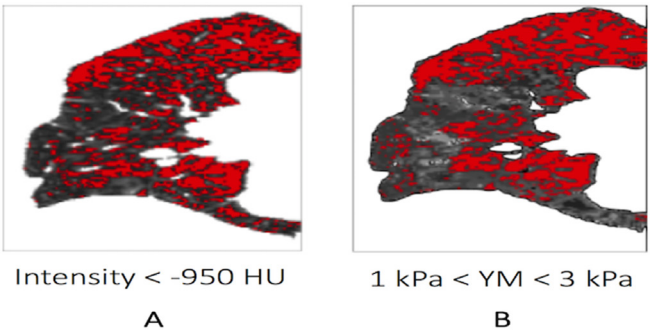

Patients with confirmed COPD are denoted with a red asterisk, while patients with normal lung function are denoted with a blue dot. Figure 5a shows the average RA_{950} value for each patient. We adopted a 5% value of average RA_{950} as a threshold for densitometrically defined emphysema.[34–36] Figure 5b shows the average YM_{1-3} for each patient, with the same patient labels as in Figure 5(a). A threshold YM_{1-3} of 2% was empirically derived to define emphysema. The upper left quadrant of each figure illustrates the true positives, the right upper quadrant illustrates false positives, the lower left quadrant illustrates false negatives, and the lower right quadrant illustrates true negatives. It can be seen that using a diagnostic criteria derived from RA_{950} results in only 4 true positives, while the remaining COPD patients are misclassified as non-COPD. Conversely, using the elasticity diagnostic criteria, 7 of the 8 COPD patients are correctly classified. All non-COPD patients are correctly classified with RA_{950} while 1 non-COPD patient is misclassified with the elasticity metric.

The statistical measures used to evaluate the two metrics are shown in Table 4. The YM_{1-3} metric had a significantly ($p < 0.05$) higher accuracy than RA_{950}. YM_{1-3} was more sensitive as a COPD metric than RA_{950}, but RA_{950} was more specific. Specificity describes the extent to which reported positives represent the condition of interest. YM_{1-3} was less specific than RA_{950} because of the patient who would be falsely identified as COPD-positive, seen in the upper right quadrant of Figure 5b. To evaluate a single metric independent of threshold, the area under the ROC curve (AUROC) was investigated and is also listed in Table 4. The AUROC is higher for YM_{1-3} when compared to RA_{950}, which indicated that, for the cases evaluated here, YM_{1-3} classified the patient cases better than the conventional densitometric metric, RA_{950}. This demonstrates that the elasticity is a superior indicator of the underlying lung pathophysiology.

Figure 5. (a) RA950 for each patient and (b) YM_{1-3} for each patient. Patients with confirmed COPD are denoted with red stars.

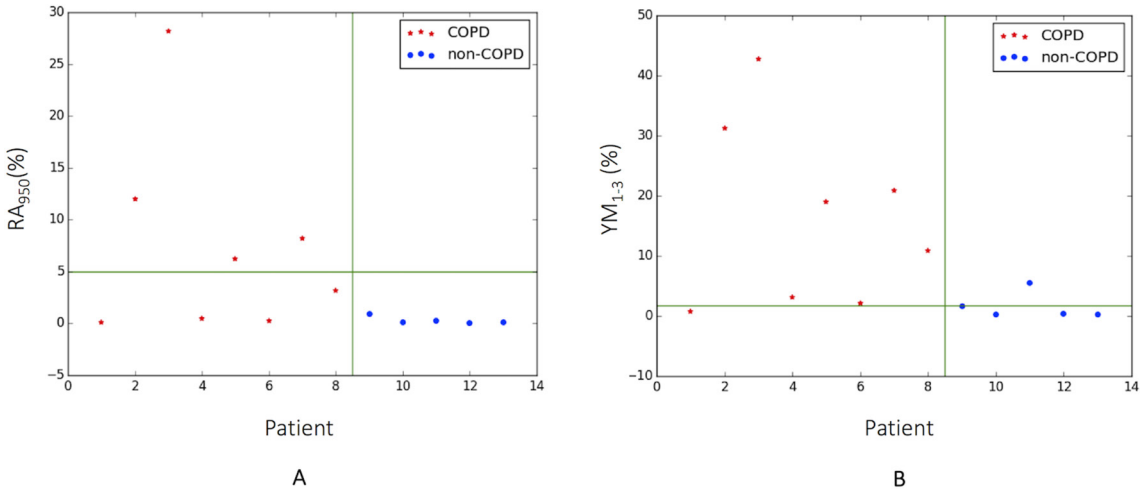

In summary, the aforementioned three experiments demonstrate the ability of lung tissue elasticity to serve as a spatial quantification of disease extent. Furthermore, we demonstrated the ability of the mechanics-based imaging biomarker YM_{1-3} to guide the diagnosis and staging procedures for COPD patients.

DISCUSSION

In this article, we investigated lung tissue elasticity as a potential imaging biomarker for COPD diagnosis using a set of 13 patients. Accuracy of the elasticity estimation was demonstrated by the high convergence percentages. The elasticity distributions allowed for the depiction of functional lung regions based on lung deformation biomechanics. Future work will investigate mapping the elasticity values to specific structures in the lung and evaluating changes for patients at various GOLD stages. This information has the potential to be used for the early detection of GOLD 1 disease. Furthermore, a the elasticity information was translated into a mechanics-based biomarker (YM_{1-3}) that was investigated in this article for evaluating disease staging and progression, with results similar to and exceeding that of RA_{950} based scoring of COPD.

While the novel mechanics-based metric shows great promise for COPD diagnosis and staging, we would like to highlight two limitations of the current work. First, the input data stems from 4DCT scans of lung cancer radiotherapy patients. The accuracy of the metric will depend on the accuracy and reproducibility of the 4DCT technique. Furthermore, 4DCT is not conventionally used for COPD patients because of its inherently high imaging dose.

Table 4. Statistical measures used to analyze prediction accuracy of the conventional RA_{950} versus YM_{1-3}

	RA_{950}	YM_{1-3}
Accuracy	0.7142	0.8571
Sensitivity	0.5	0.875
Specificity	1	0.833
AUROC	0.875	0.917

The lesions of the lung cancer patients might also further affect the results. Currently, SPIROMICS studies have employed an effective imaging dose of 3.2 mSv in their protocols for acquiring the total lung capacity.[37] We anticipate that with an increasing scope of application for 4DCT in COPD diagnosis and staging, imaging experts will focus on reducing the imaging dose to a level that is within the imaging limits for COPD. For instance, prospective and low dose scanning techniques are being investigated by peers for reducing the 4DCT imaging dose. Once the dose can be reduced for the assessment of COPD, the scans can be used for a longitudinal assessment of COPD progression and better differentiation of the degree and type of COPD. Elastography methods using deformation seen between RV and TLC lung datasets are also being investigated.

Second, the biomechanical model employs a linear elastic approach for the lung elastography. While the linear elastic model is shown to be applicable for COPD lung during normal breathing, we anticipate that for representing the full range of breathing motion, we will need to employ a hyperelastic process.[38] In future studies, the linear elastic assumptions will be expanded to hyperelastic constitutive laws. Furthermore, as MR elastography techniques mature and become more applicable to the lungs, the model-guided elastography will be validated and the YM_{1-3} metric will need to be updated accordingly.

From a radiotherapy perspective, the development of functional tissue-sparing treatment plans guided by the elasticity information will be investigated. A limitation of the patient datasets used in this study is the small sample size that was collected in a radiotherapy setting, so functional information was a byproduct of the radiology reports and no data was available as a healthy control. Future work will focus on collecting and analyzing mainstream COPD data to further evaluate the diagnostic potential. Furthermore, we will investigate the development of a clinical protocol to focus on explicitly validating lung regions affected by COPD, both emphysema and small airways disease, with a pulmonary radiologist.

In summary, a novel imaging biomarker was developed using a physics-based biomechanical model and 4DCT-driven lung elastography. A preliminary imaging biomarker for COPD was assessed in comparison to the conventional RA_{950} and performed favorably. The resultant elasticity distributions gained from our methodology can be used to identify functional regions of parenchymal tissue, leading to patient-specific treatment options and guiding pulmonary physicians as to the early management of COPD.

ACKNOWLEDGMENT

This material is supported by the National Science Foundation Graduate Research Fellowship under Grant No. DGE-1144087 and the UCLA Department of Radiation Oncology.

REFERENCES

1. Asia Pacific COPD Roundtable Group Global Initiative for Chronic Obstructive Lung Disease strategy for the diagnosis, management and prevention of chronic obstructive pulmonary disease: an Asia-Pacific perspective. *Respirology* 2005; **10**: 9–17. doi: https://doi.org/10.1111/j.1440-1843.2005.00692.x
2. Jögi J, Ekberg M, Jonson B, Bozovic G, Bajc M. Ventilation/perfusion SPECT in chronic obstructive pulmonary disease: an evaluation by reference to symptoms, spirometric lung function and emphysema, as assessed with HRCT. *Eur J Nucl Med Mol Imaging* 2011; **38**: 1344–52. doi: https://doi.org/10.1007/s00259-011-1757-5
3. Barker BL, Brightling CE. Phenotyping the heterogeneity of chronic obstructive pulmonary disease. *Clin Sci* 2013; **124**: 371–87. doi: https://doi.org/10.1042/CS20120340
4. Bhatt SP, Bodduluri S, Newell JD, Hoffman EA, Sieren JC, Han MK, et al. CT-derived biomechanical metrics improve agreement between spirometry and emphysema. *Acad Radiol* 2016; **23**: 1255–63. doi: https://doi.org/10.1016/j.acra.2016.02.002
5. Duman IE, Cimsit C, Yildizeli SO, Cimsit NC. Parenchymal density changes in acute pulmonary embolism: Can quantitative CT be a diagnostic tool? A preliminary study. *Clin Imaging* 2017; **41**: 157–63. doi: https://doi.org/10.1016/j.clinimag.2016.11.005
6. Kirby M, Pike D, Sin DD, Coxson HO, McCormack DG, Parraga G. COPD: Do imaging measurements of emphysema and airway disease explain symptoms and exercise capacity? *Radiology* 2015; **277**: 872–80. doi: https://doi.org/10.1148/radiol.2015150037
7. Wielpütz MO, Bardarova D, Weinheimer O, Kauczor HU, Eichinger M, Jobst BJ, et al. Variation of densitometry on computed tomography in COPD--influence of different software tools. *PLoS One* 2014; **9**: e112898. doi: https://doi.org/10.1371/journal.pone.0112898
8. Regan EA, Hokanson JE, Murphy JR, Make B, Lynch DA, Beaty TH, et al. Genetic epidemiology of COPD (COPDGene) study design. *COPD* 2010; **7**: 32–43. doi: https://doi.org/10.3109/15412550903499522
9. Parr DG. Quantifying the lung at risk in chronic obstructive pulmonary disease. Does emphysema beget emphysema? *Am J Respir Crit Care Med* 2017; **196**: 535–6. doi: https://doi.org/10.1164/rccm.201705-0962ED
10. Crossley D, Renton M, Khan M, Low EV, Turner AM. CT densitometry in emphysema: a systematic review of its clinical utility. *Int J Chron Obstruct Pulmon Dis* 2018; **13**: 547–63. doi: https://doi.org/10.2147/COPD.S143066
11. Mascalchi M, Camiciottoli G, Diciotti S. Lung densitometry: why, how and when. *J Thorac Dis* 2017; **9**: 3319–45. doi: https://doi.org/10.21037/jtd.2017.08.17
12. Galbán CJ, Han MK, Boes JL, Chughtai KA, Meyer CR, Johnson TD, et al. Computed tomography-based biomarker provides unique signature for diagnosis of COPD phenotypes and disease progression. *Nat Med* 2012; **18**: 1711–5. doi: https://doi.org/10.1038/nm.2971
13. Boes JL, Hoff BA, Bule M, Johnson TD, Rehemtulla A, Chamberlain R, et al. Parametric response mapping monitors temporal changes on lung CT scans in the subpopulations and intermediate outcome measures in COPD Study (SPIROMICS). *Acad Radiol* 2015; **22**: 186–94. doi: https://doi.org/10.1016/j.acra.2014.08.015
14. Risholm P, Ross J, Washko GR, Wells WM. Probabilistic elastography: estimating lung elasticity. *Inf Process Med Imaging* 2011; **22**: 699–710.
15. Cotes JE, Chinn DJ, Miller MR. Lung function: physiology, measurement and application in medicine. In: . *6th ed*. Malden, Mass, *Oxford*: Blackwell Pub; 2006. pp. 636.
16. Ionescu C, Derom E, De Keyser R. Assessment of respiratory mechanical properties with constant-phase models in healthy and COPD lungs. *Comput Methods Programs Biomed* 2010; **97**: 78–85. doi: https://doi.org/10.1016/j.cmpb.2009.06.006
17. MacNee W. Pathogenesis of chronic obstructive pulmonary disease. *Clin Chest Med* 2007; **28**: 479–513. doi: https://doi.org/10.1016/j.ccm.2007.06.008
18. Marinelli JP, Levin DL, Vassallo R, Carter RE, Hubmayr RD, Ehman RL, et al. Quantitative assessment of lung stiffness in patients with interstitial lung disease using MR elastography. *J Magn Reson Imaging* 2017; **46**: 365–74. doi: https://doi.org/10.1002/jmri.25579
19. Pepin KM, Ehman RL, McGee KP. Magnetic resonance elastography (MRE) in cancer: Technique, analysis, and applications. *Prog Nucl Magn Reson Spectrosc* 2015; **90-91**: 32–48. doi: https://doi.org/10.1016/j.pnmrs.2015.06.001
20. Negahdar M, Fasola CE, Yu AS, von Eyben R, Yamamoto T, Diehn M, et al. Noninvasive pulmonary nodule elastometry by CT and deformable image registration. *Radiother Oncol* 2015; **115**: 35–40. doi: https://doi.org/10.1016/j.radonc.2015.03.015
21. Weiss E, Wijesooriya K, Dill SV, Keall PJ. Tumor and normal tissue motion in the thorax during respiration: Analysis of volumetric and positional variations using 4D CT. *Int J Radiat Oncol Biol Phys* 2007; **67**: 296–307. doi: https://doi.org/10.1016/j.ijrobp.2006.09.009
22. Rietzel E, Pan T, Chen GT. Four-dimensional computed tomography: image formation and clinical protocol. *Med Phys* 2005; **32**: 874–89. doi: https://doi.org/10.1118/1.1869852
23. Werner R, Ehrhardt J, Schmidt R, Handels H. Patient-specific finite element modeling of respiratory lung motion using 4D CT image data. *Med Phys* 2009; **36**: 1500–11. doi: https://doi.org/10.1118/1.3101820
24. Hasse K, Neylon J, Santhanam AP. Feasibility and quantitative analysis of a biomechanical model-guided lung elastography for radiotherapy. *Biomed Phys Eng Express* 2017;

3: 025006. doi: https://doi.org/10.1088/2057-1976/aa5d1c

25. Thomas D, Lamb J, White B, Jani S, Gaudio S, Lee P, et al. A novel fast helical 4D-CT acquisition technique to generate low-noise sorting artifact-free images at user-selected breathing phases. *Int J Radiat Oncol Biol Phys* 2014; **89**: 191–8. doi: https://doi.org/10.1016/j.ijrobp.2014.01.016
26. Wang J, Li F, Li Q. Automated segmentation of lungs with severe interstitial lung disease in CT. *Med Phys* 2009; **36**: 4592–9. doi: https://doi.org/10.1118/1.3222872
27. Neylon J, Qi X, Sheng K, Staton R, Pukala J, Manon R, et al. A GPU based high-resolution multilevel biomechanical head and neck model for validating deformable image registration. *Med Phys* 2015; **42**: 232–43. doi: https://doi.org/10.1118/1.4903504
28. Gao L, Parker KJ, Lerner RM, Levinson SF. Imaging of the elastic properties of tissue--a review. *Ultrasound Med Biol* 1996; **22**: 959–77. doi: https://doi.org/10.1016/S0301-5629(96)00120-2
29. Min Y, Neylon J, Shah A, Meeks S, Lee P, Kupelian P, et al. 4D-CT Lung registration using anatomy-based multi-level multi-resolution optical flow analysis and thin-plate splines. *Int J Comput Assist Radiol Surg* 2014; **9**: 875–89. doi: https://doi.org/10.1007/s11548-013-0975-7
30. Hasse K, O'Connell D, Min Y, Neylon J, Low DA, Santhanam A. Estimation and validation of patient-specific high-resolution lung elasticity derived from 4DCT. *Med Phys* 2018; **45**: 666–77. doi: https://doi.org/10.1002/mp.12697
31. Hering T. Update of the GOLD-recommendations - new strategy in diagnostics and therapy of COPD. *MMW Fortschr Med* 2017; **159**: 53–4. doi: https://doi.org/10.1007/s15006-017-9391-1
32. Papaioannou M, Pitsiou G, Manika K, Kontou P, Zarogoulidis P, Sichletidis L, et al. COPD assessment test: a simple tool to evaluate disease severity and response to treatment. *COPD* 2014; **11**: 489–95. doi: https://doi.org/10.3109/15412555.2014.898034
33. Marks LB, Bentzen SM, Deasy JO, Kong FM, Bradley JD, Vogelius IS, et al. Radiation dose-volume effects in the lung. *Int J Radiat Oncol Biol Phys* 2010; **76**(3 Suppl): S70–S76. doi: https://doi.org/10.1016/j.ijrobp.2009.06.091
34. Camiciottoli G, Cavigli E, Grassi L, Diciotti S, Orlandi I, Zappa M, et al. Prevalence and correlates of pulmonary emphysema in smokers and former smokers. A densitometric study of participants in the ITALUNG trial. *Eur Radiol* 2009; **19**: 58–66. doi: https://doi.org/10.1007/s00330-008-1131-6
35. Gevenois PA, De Vuyst P, Sy M, Scillia P, Chaminade L, de Maertelaer V, et al. Pulmonary emphysema: quantitative CT during expiration. *Radiology* 1996; **199**: 825–9. doi: https://doi.org/10.1148/radiology.199.3.8638012
36. Kauczor HU, Hast J, Heussel CP, Schlegel J, Mildenberger P, Thelen M. CT attenuation of paired HRCT scans obtained at full inspiratory/expiratory position: comparison with pulmonary function tests. *Eur Radiol* 2002; **12**: 2757–63. doi: https://doi.org/10.1007/s00330-002-1514-z
37. Yin Y, Raffy P, Sieren JP, Newell JD, Hoffman EA. Quantitative CT In spiromics: lobar evaluation via image warping Of tlc masks onto Rv images. *Am J Respir Crit Care Med* 2014; **189**: A4332.
38. Agusti AGN. Systemic effects of chronic obstructive pulmonary disease. *Proc Am Thorac Soc* 2005; **2**: 367–70. doi: https://doi.org/10.1513/pats.200504-026SR